ADVANCED FUNCTIONAL MATERIALS
www.afm-journal.de

First-Principles Design of Ohmic FET Devices from 2D Transition Metal Dichalcogenides

Zahra Golsanamlou, Alessandro Fortunelli, and Luca Sementa**

A chlorine-doped ultrathin phase of hafnium disulfide (HfS_2) is proposed as an ideal candidate material for 2D field-effect transistor (FET) device applications, down to the extreme sub-5 nm miniaturization limit. This transition metal dichalcogenide 2D material is designed to combine features of both a metal and a semiconductor, exhibiting a high electric conductivity comparable with ordinary metals, that can be abruptly cut down via gating due to an energy gap immediately below the Fermi level and its anomalous metallic properties. These unique features enable realizing an alternative design of a FET device in which electrode and channel are made of the same Cl-doped ML HfS_2 phase, a potential breakthrough bypassing all issues associated with electronic (Schottky) and structural dis-homogeneities or low conductivity that have hindered progress in this field. This material/design combination shall lead to a FET device with purely ohmic behavior, high metallic conductance, no interfacial contact resistance, and facile gating with extremely high on/off ratio.

1. Introduction

2D transition metal dichalcogenides (TMDCs) have attracted enormous attention due to easy preparation in 2D form, e.g., via exfoliation,[1] and features uniquely favorable for applications in spintronics,[2,3] optoelectronics,[4,5] catalysis,[6,7] and energy storage devices,[8,9] either individually,[10–13] or combined with other 2D materials in lateral (LH)[14,15] or vertical heterostructures (VH).[16] One of the breakthrough perspective applications of 2D TMDCs is as field-effect transistors (FETs). Their electronic, chemical, and mechanical properties[17,18] combined with ultrathin dimension open the way to the ultimate size limit for conducting/semiconducting junctions, promising to surpass present silicon-based integrated circuit technology and finally enabling the long-sought sub-5-nm FET miniaturization.[2,10,12]

In TMDC FETs proposed so far, a metal TMDC is combined with a semiconductor TMDC to enable on and off tuning of electric conduction via gating.[12] The hetero-junction is a critical component of such a FET, as it governs charge injection from the electrode into the channel. However, the phenomenon of Fermi level pinning (FLP) at the interface, with the creation of a Schottky barrier (SB),[19] significantly degrades device performance and efficiency, and represents a major issue in FET design. Many efforts have been devoted to reduce the SB height (SBH),[17,20,21] ideally aiming at achieving a purely ohmic contact (zero SBH), exploiting band-structure engineering,[22–24] buffer layer[17,25,26] reducing the density of metal-induced gap states (MIGS),[27,28] doping,[24,29–32] or vacancies,[33] but with no practical solution so far. A further major issue associated with a hetero-structure is the requirement that transfer matrix elements at the interface are large, i.e., high hybridization between orbitals in the metal and in the semiconductor.[13,20,34] Finally but equally importantly, values of electric conduction in TMDCs are typically low since electronic transmission occurs in the narrow valence *d*-band.

Here, we explore an alternative, potentially breakthrough design. We carefully construct a unique TMDC 2D phase which combines features of both a highly conducting metal and a semiconductor and propose a FET device in which on and off tuning of electric conduction is achieved by employing such a single 2D material. Our proposal thus completely bypasses all issues connected with the SB, all structural compatibility problems at the metal/semiconductor interface, as well as the low conductivity that plagues the TMDC-based FETs proposed so far. Specifically, we single out a chlorine(Cl)-doped monolayer (ML) 1T phase of the hafnium disulfide (HfS_2) TMDC semiconductor, and we demonstrate via first-principles electronic structure and transport simulations that this material simultaneously possesses: i) a high density of transmitting electronic states at the Fermi level, with a conductivity comparable to metals like copper, since electronic transmission occurs in the conduction band;

Z. Golsanamlou, L. Sementa
CNR-IPCF
Consiglio Nazionale delle Ricerche
via G. Moruzzi 1, Pisa 56124, Italy
E-mail: luca.sementa@cnr.it

A. Fortunelli
CNR-ICCOM
Consiglio Nazionale delle Ricerche
via G. Moruzzi 1, Pisa 56124, Italy
E-mail: alessandro.fortunelli@cnr.it

The ORCID identification number(s) for the author(s) of this article can be found under https://doi.org/10.1002/adfm.202310077

DOI: 10.1002/adfm.202310077

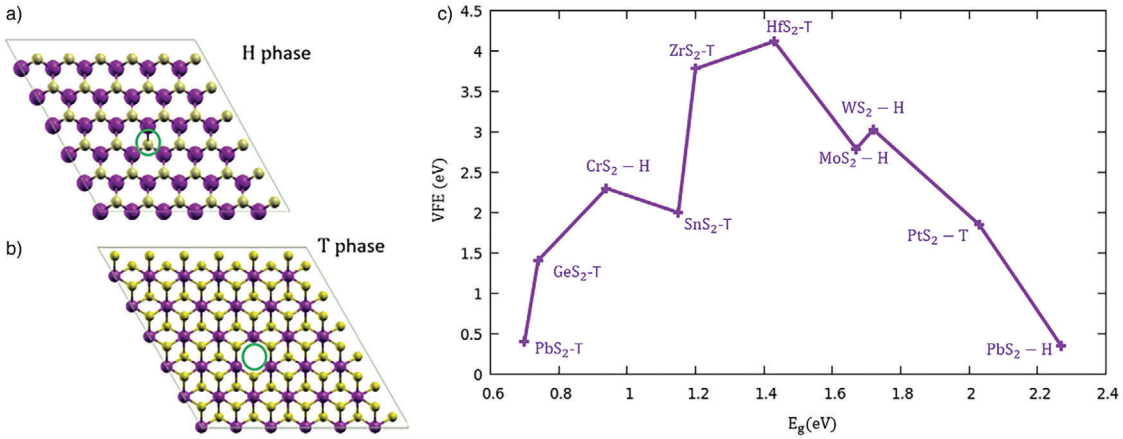

Figure 1. a) 6 × 6 hexagonal super cell with one S vacancy in the H phase, b) 6 × 6 hexagonal super cell with one S vacancy in T phase; in both figures the green circles indicate the S vacancy site, and c) vacancy formation energy (VFE) for several TMS_2 as a function of the bandgap.

ii) an energy gap immediately below the Fermi level, a unique feature that, combined with the anomalous character of this 2D metal, should enable facile gating effects. We thus advocate that a FET in which electrode and channel are made of the same Cl-doped ML 1T HfS_2 material will behave as a purely ohmic contact with zero SB or interfacial resistance and extremely high on/off ratios, thus representing an ideal candidate for FET nanodevice applications. We support and rationalize our design results via an analysis of the origin and characteristics of mid-gap states (MGS) in ML HfS_2 with sulfur(S) vacancies or chlorine dopants, providing the basis for further extensions of our approach.

First-principles atomistic simulations for predicting both structural and transmission properties were performed using the density functional theory (DFT)[12,13] (we refer to Section 4 for a detailed description of the Computational Approach). After analyzing many TMDCs systems, we select HfS_2 as the most promising candidate based on thermodynamic and electronic structure properties (high vacancy formation energy and correspondingly shallow defect/vacancy states).

2. Results and Discussion

As discussed hereafter we start by calculating the formation energy of sulfur (S) vacancies in the semiconductor for a set of TMDCs, using a 6 × 6 hexagonal supercell replicating the TMDC minimal unit cell (see **Figure** 1a,b for different phases of hexagonal supercell).[35] The vacancy formation energy (VFE) for the selected systems is given in Figure 1c, calculated via the formula:

$$VFE = E^{TMS_2} - \left(E_{perfect}^{TMS_2} - N \times E_{TM,S}^{free-atoms}\right) \quad (1)$$

where E^{TMS_2} and $E_{perfect}^{TMS_2}$ refer to the total energies of defective and perfect TMS_2 ML, respectively, N is the number of removed atoms, and $E_{TM,S}^{free-atoms}$ is the energy of TM or S atoms in a chemically stable reference state. HfS_2 and ZrS_2 turn out to have the highest VFE among the investigated TMS_2 ML phases. Notably, in these semiconductors the S vacancy creates a filled state right below the bottom of the conduction band (BCB shallow defect states), as apparent in Figure S1b (Supporting Information) for HfS_2, whereas for TMS_2 semiconductors with moderate or small VFE, the S vacancy creates a deep gap state,[30] see Figure S3 (Supporting Information) for PdS_2 as an example.

Figure 2a,b show the top view of the HfS_2 ML in the 1T phase with and without S vacancies, respectively. The length of the system in the transport direction is 100.8 Å and in the perpendicular direction is 7.24 Å.

The filled states created by sulfur vacancies right below the BCB ensure that vacancy-defected HfS_2 becomes metallic (see Figure S1b, Supporting Information), with the Fermi level

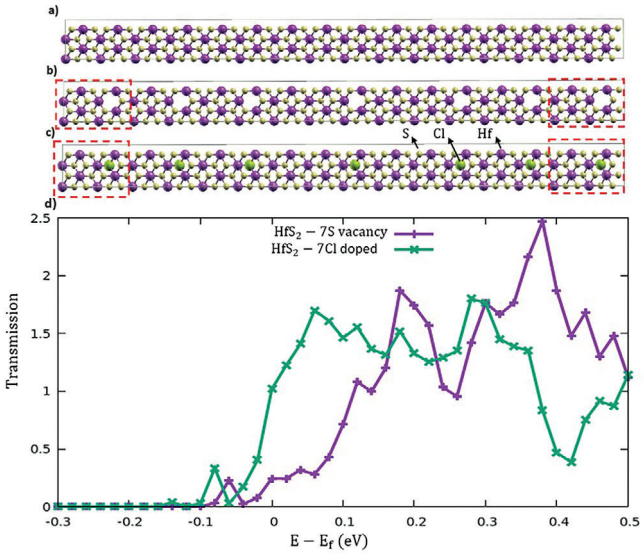

Figure 2. a) perfect 1T HfS_2 ML, b) 1T HfS_2 ML in the presence of S vacancies, c) chlorine (Cl)-doped 1T HfS_2 ML, and d) transmission coefficient of 1T HfS_2 in the presence of S vacancies (magenta curve) or Cl dopants (green curve). The red rectangular boxes in panels (a-c), whose longest edges are about 12.5 Å, show the leads used in the transmission simulations. Taken as a whole, the scattering region and the leads measure 100.8 Å.

located close to the vacancy states and an electronic energy gap immediately below. Such a system will behave like a metal around E_f, but with a conduction abruptly going to zero below the Fermi level, i.e., it achieves our target for building a FET device using a single 2D TMDC material. Indeed, results of transmission simulations (a reliable tool to investigate SBH computationally)[21] confirm this expectation, as illustrated in Figure 2d where the transmission coefficient of HfS_2 ML with S vacancies is reported as the curve in magenta. The finite transmission at E_f and in a small interval below E_f indicating a zero SBH should be noted. The idea guiding our design is that semiconductors with a higher vacancy formation energy (VFE) are better starting points for introducing S vacancy defects, because in these systems S vacancies create delocalized states close to the BCB, whereas in semiconductors with lower VFE the vacancy states are localized and can act as scattering centers for charge transport. To prove this, we investigated a PdS_2 1T TMDC ML, which has a lower VFE and in which sulfur vacancy states lie in the middle of the bandgap (as illustrated in Figure S3, Supporting Information), and found that PdS_2 still exhibits FLP and SB phenomena, see Figure S8 (Supporting Information). HfS_2 and ZrS_2 are thus selected for further investigation of transport properties in the presence of dopants (note that Hf and Zr belong to the same column of the periodic table).

Experimentally, sulfur vacancies in TMDCs can be produced by modifying the synthesis parameters, or using an electron beam.[36] However, the presence of atomic vacancies and unsaturated bonds destroys one of the main advantages of TMDCs as 2D materials, which is the absence of dangling bonds, creating chemical stability issues in practical electronic devices. This prompted us to explore chlorine doping (i.e., "curing" the S vacancies with Cl atoms) to increase the chemical stability of the system. Cl-doping will simultaneously also increase the density of states (DOS) at the Fermi level as we are adding an atom (chlorine) with one electron more than the removed sulfur. In other words, Cl-doping should further populate the bottom of the conduction band with high-mobility electrons whose effective mass is low due to extended conjugation, without modifying the wide bandgap below the Fermi level, therefore further improving the suitability of the material for FET applications. Note also that chlorine comes right after sulfur in the periodic table, so its similar atomic size should not create thermodynamic penalties and geometric strain due to size mismatch. Results of DOS calculations in Figure S1d (Supporting Information) confirm that Cl-doped HfS_2 exhibits a filled state right below the BCB and is metallic. Moreover, the reaction energy ΔE for the replacement of S with Cl, defined as:

$$E\left(HfS_2\right) + \frac{1}{2}Cl_2 \rightarrow E\left(Cl-\text{doped}HfS_2\right) + \frac{1}{32}S_{32} \quad (2)$$

reads −0.1 eV, which proves the thermodynamic stability of the doped system. Indeed, it is experimentally proven that Cl doping can be achieved by exposing TMDC MLs to Cl_2 gas.[37] Finally, Figure 2d shows that filling the vacancies with Cl atoms improves the transmission coefficient around the Fermi level up to metallic values and that the transmission exhibits a quasi-ohmic behavior. Indeed, the transmission of Cl-doped HfS_2 is comparable with that of metals like Cu (see Figure S5, Supporting Information). Moreover, the fact that carriers do not face any barrier entails ohmic behavior and should lead to a high on–off ratio for FET current.[38,39]

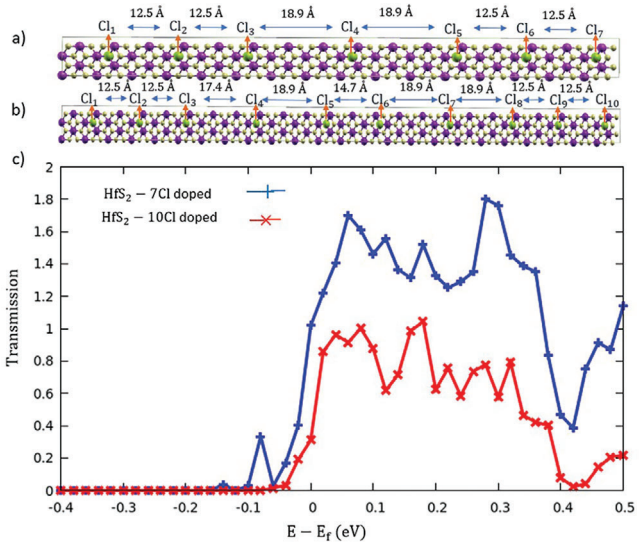

Figure 3. a) Asymmetrically doped HfS_2 (1T) ML with 7Cl atoms at shorter distance, b) asymmetrically doped HfS_2 (1T) ML with 10 Cl atoms at larger distance, and c) transmission coefficient for the Cl-doped systems defined in a) and b). Note that the total length of the system in b) is larger than the total length of the system i The doped-HfS_2 unit cell employed as a lead is like the ones illustrated within the red boxes of Figure 2.

A perusal of previous experiments provides hints that support our contention. For example, the contact resistance of a metal(Ni–Au)/semiconductor(MoS_2/WS_2) interface was decreased using chlorine molecular doping.[27] In that work the authors considered few-layers MoS_2 and WS_2 systems, because in the MoS_2 and WS_2 monolayers the states created by Cl-doping are far from both the top of the valence band (TVB) and the BCB, are localized, and act as scattering centers for transport,[30] whereas increasing the number of layers of MoS_2 and WS_2 reduces the bandgap,[22] favors the matching of the defect states to one of the band edges (TVB or BCB), and also favors hybridization which in turn increases delocalization and carrier mobility and reduces the contact resistance.

For practical applications, it is interesting to test whether the transmission is robust with respect to the density of dopants, also considering that the length of the channel in experiments may be more than 10 nm. To this end, we first verified that when the channel assumes the geometry of the leads, so that the scattering region hosts defects homogeneously distributed with a distance of 12.53 Å, even doubling the length of the channel does not deteriorate the transmission properties (see right-hand panel of Figure S5, Supporting Information). In contrast, the transmission does depend on the distance between the dopant Cl atoms. **Figure 3** reports the transmission coefficient for two different distributions of Cl-dopants in HfS_2. In the former one (Figure 3a) the system has a total length of 100.8 Å along the transport direction and the distance between Cl atoms of the scattering region is 18.9 Å, which is about 6.4 Å larger than the one in the leads. In

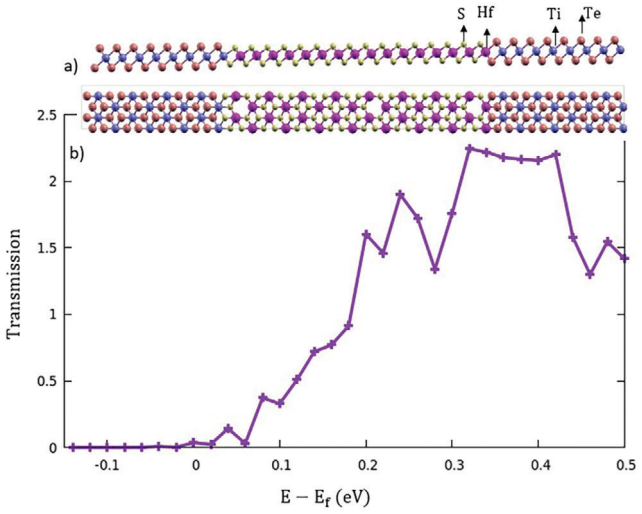

Figure 4. a) Side and top view of $TiTe_2/HfS_2$ LH in the presence of S vacancies, and b) transmission coefficient of $TiTe_2/HfS_2$ LH in the presence of S vacancies. The $TiTe_2$ unit cell we assumed as a lead extends about 6.5 A along the transmission direction. The device's total length (scattering + leads) is ≈100.5 A

the latter one (Figure 3b) the system exhibits a scattering region 60% longer than in the former one (total length of 150.4 Å along the transport direction) with a distance between defects ranging from 12.53 to 18.9 Å. The results in Figure 3 show that, increasing the channel length in the presence of defect inhomogeneity, somewhat deteriorates the transmission, which however remains sizable for a system whose length is comparable with the ones attainable experimentally. These results can be rationalized by analyzing the charge distribution of the electronic states at the TVB of the Cl-doped system (Figure S4, Supporting Information). The TVB states are centered around the Cl dopants, however the lower the Cl–Cl distance the larger is the charge spreading. Thus, if the dopant density (therefore, the carrier density) is high enough, the tails of the wave functions of the valence Cl states will interact with each other to produce delocalized states to thus yield an efficient electron transmission. On the contrary, when the Cl atoms are farther from each other, as in the center of Figure S4 (Supporting Information), the states become more localized around the dopant, increasing the height of the potential barrier experienced by the conduction electrons (the system becomes like a semiconductor).

We can explore further variations of the strategy here proposed. For example, we can employ a metallic TMDC as a lead and interface it with a defected HfS_2 as a channel, obtaining a more customary source/drain device based on 2D heterostructures.[12] Among possible TMDCs, we found that $TiTe_2$ exhibits a quasi-perfect alignment between its work function with the BCB of defected HfS_2 (difference of only 0.05 eV), and also a lattice mismatch of ≈2% leading to minimal structural strain at the interface, suggesting good carrier injection not strongly affected by corrugation phenomena. Indeed, **Figure 4** shows that a $TiTe_2/HfS_2$ hetero-structure has transmission properties comparable with those of the HfS_2-defected system. Furthermore, by inspecting Figure S7 (Supporting Information) it appears that introducing S-vacancies within the HfS_2 ML improves the transmission and eliminates the 0.37 eV SB at the defect-free $HfS_2/TiTe_2$ interface. Finally, recalling that a transmission that is constant with bias yields a linear *I–V* curve,[40] and noting that the transmission of the defected-$HfS_2/TiTe_2$ heterostructure reported in Figure 4b is hardly affected by the potential bias within the range 0.3–0.4 eV above E_f, we predict that, by bringing the Fermi level into this energy range using a proper gate voltage, one can obtain a device with linear *I–V* characteristics similar to the ohmic response of metallic systems like Cu.

Further expanding on the approach here proposed, we explored cation vacancies or better cation doping rather than chalcogen doping. Although the formation energy of a metal vacancy in TMDCs is higher than that of a chalcogen vacancy,[41,42] the presence of a metal vacancy or of a metal dopant with one electron less than the original metal element can create holes in the valence band, thus increasing the number of carriers without affecting the energy gap, a fact which is potentially beneficial for FET applications. TMs with one electron less than Hf in the periodic table belong to the lanthanide series, and their *f*-electrons introduce a further degree of freedom. Thus, to explore this avenue in pure form we considered ZrS_2 instead of HfS_2. Zr and Hf belong to the same column of the periodic table, and ZrS_2 and HfS_2 share similar properties. Indeed, Figure S6 (Supporting Information) shows that HfS_2 and ZrS_2 have similar transmission after introducing a S vacancy, while Figures S1c and S2b (Supporting Information), respectively, indicate similar DOS for HfS_2 and ZrS_2 MLs exhibiting a cation vacancy. Zr has the advantage that we can replace Zr with yttrium (Y) in the ZrS_2 ML 1T phase to explore metal cation doping. **Figure 5** shows the transmission coefficient for p-doped ZrS_2 in the presence of a Zr vacancy or Zr → Y replacement. As it is clear from Figure 5c, Y doping appreciably improves the transmission coefficient around and

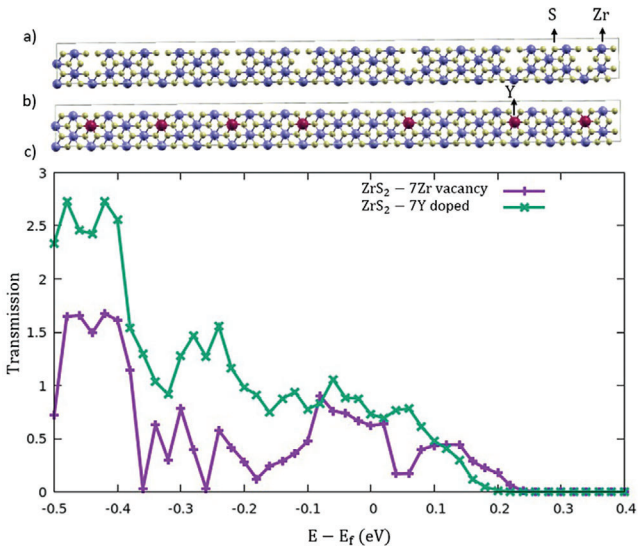

Figure 5. a) ZrS_2 ML with metal vacancies, b) ZrS_2 ML with Y dopants, and c) transmission coefficient in the presence of metal vacancies (magenta curve) or Y dopants (green curve). The longest edge of the ZrS_2 rectangular unit cell we used as lead is ≈12.6 Å. whereas the device's total length is ≈102 Å.

below the Fermi level, and the metallic character of the system. As both metal vacancy and a p-dopant create an empty state right above the TVB, we find a non-zero transmission coefficient for holes below the Fermi level, so that the transmission becomes ohmic due to nonzero transmission at and above E_f. A p-doped ZrS_2 ML obtained via Zr-vacancy or better Y-doping is thus an alternative way to realize a single-phase electrode/channel FET material.

To conclude this section, we briefly discuss possible issues in experimentally realizing the proposed devices. First, transmission may be negatively affected by doping, and limited by achievable charge carrier density. However, a previous study[43] on MoS_2 suggests that the mobility reduction caused by ionized dopants is negligible in comparison to other conductivity-degrading scattering processes, such as phonon scattering, whose impact usually increases with temperature. As for charge carrier density, our calculations indicate that the doped HfS_2 system has a 2D carrier density of 1.1×10^{14} electrons cm^{-1},[2] which is only one order of magnitude lower than the 2D carrier density of the Cu stripe (3.0×10^{15} electrons cm^{-2}), whose calculated transmission we used as a term of comparison. In any case, experimental validation of the proposed material will probably require fine tuning of the synthesis procedure. Moreover, while 2D semiconductor doping has been explored so far for scientific purposes, upscaling the production of high-quality and uniformly 2D doped semiconductors and integrating the 2D FET devices into the existing technology remain significant challenges that would demand concerted efforts from diverse fields.

3. Conclusion

In the present work we rationally designed via first principles modeling a Cl-doped monolayer (ML) 1T phase HfS_2 as an ideal candidate for realizing 2D FET devices. This unique material should enable realizing an alternative and potentially breakthrough approach to FETs, in which the same material is employed as both the electrode and the channel. Electronic structure and transport simulations demonstrate that the proposed material behaves as an anomalous conductor with unique features, exhibiting simultaneously a large density of conducting electronic states at the Fermi level and an energy gap immediately below it. This simultaneously leads to large values of purely ohmic transmission (no SB nor structural compatibility issues at hetero-structure interfaces), and a facile gating with a potentially extremely high on/off ratio (high electric transmission around E_f comparable with metals like copper giving the way to zero transmission in the underlying energy gap, together with imperfect metallic screening that enables gating a metallic system). We justify our proposal and rationalize the observed behavior by analyzing S vacancies in HfS_2, and how the associated mid-gap states (MGS) evolve upon doping/substituting sulfur anions. Additionally, we test the stability of the proposed material to fluctuations in the density of dopants, we propose $TiTe_2$ ML phase as a good metal contact with defected HfS_2 in a hetero-structure junction, and we explore cation vacancy or doping as an alternative to realize the strategy here proposed. The present results should open a new avenue to the realization of optoelectronic devices at the extreme limit of miniaturization.

4. Computational Details

Geometry optimizations and electronic structure calculations are performed using density functional theory (DFT) with a plane-wave basis set, and the Perdew–Burke–Ernzerhof (PBE) gradient-corrected exchange-correlation (xc-)functional,[44] as implemented in the Quantum Espresso (QE) package.[45,46] Scalar-relativistic ultrasoft pseudopotentials (US-PPs) are utilized, employing 50 Ry as the energy cutoff for the wave function and 500 Ry as the density cutoff for the density. A $1 \times 22 \times 12$ Monkhorst-Pack k-mesh is used to sample the Brillouin zone (BZ) of the orthogonal unit cells and a $1 \times 12 \times 1$ k-mesh for the scattering system. A vacuum layer of 22 Å is used to avoid interactions with replicated unit cells. Transmission simulations are performed based on a scattering state approach considering rightward propagating modes from the left to the right electrode as implemented in the QE/PWcond routine.[47,48] The approach integrates numerically a scattering equation in real space along the direction of transport according to the formula: $T = \sum_{mn} |T_{mn}|^2 = Tr[\mathbf{T}^{+}\mathbf{T}]$where, m (n) is related to the propagating and decaying states on the left (right) leads and T is the matrix of normalized transmission amplitudes, $T_{mn} = \sqrt{\frac{I_m}{I_n}} t_{mn}$. Here, I_m and I_n are the currents carried by the state m and n, respectively. This approach employs scattering theory for rightward propagating modes from the left to the right electrode,[47] which holds in the limit of ballistic transport. The same ($1 \times 12 \times 1$) k-mesh we employed for structural relaxations is also used in transmission simulations. The left and right leads are illustrated in Figure 2b,c as enclosed by dashed lines.

Supporting Information

Supporting Information is available from the Wiley Online Library or from the author.

Acknowledgements

The authors are grateful to Poonam Kumari for interesting and useful discussions. The authors acknowledge financial support from the FIVE2D project (2017SRYEJH) within the Italian MUR-PRIN calls and the QUEFORMAL project, that received funding from the European Union's Horizon 2020 Research and Innovation Program under the H2020 Future and Emerging Technologies (FET) Open Grant Agreement No. 829035. The authors thank the ISCRA program at the Cineca supercomputer center (Bologna, Italy) for providing computational resources.

Conflict of Interest

The authors declare no conflict of interest.

Data Availability Statement

The data that support the findings of this study are available from the corresponding author upon reasonable request.

Keywords

electronic band structure, field-emission transistors, miniaturized electronic devices, rational design, transition metal dichalcogeneides

Received: August 23, 2023
Revised: November 24, 2023
Published online: December 13, 2023

[1] A. Jawaid, D. Nepal, K. Park, M. Jespersen, A. Qualley, P. Mirau, L. F. Drummy, R. A. Vaia, *Chem. Mater.* **2016**, *28*, 337.
[2] Q. H. Wang, K. Kalantar-Zadeh, A. Kis, J. N. Coleman, M. S. Strano, *Nat. Nanotechnol.* **2012**, *7*, 699.
[3] N. Cortés, O. Ávalos-Ovando, L. Rosales, P. A. Orellana, S. E. Ulloa, *Phys. Rev. Lett.* **2019**, *122*, 086401.
[4] K. F. Mak, J. Shan, *Nat. Photonics* **2016**, *10*, 216.
[5] E. Najafidehaghani, Z. Gan, A. George, T. Lehnert, G. Q. Ngo, C. Neumann, T. Bucher, I. Staude, D. Kaiser, T. Vogl, U. Hübner, U. Kaiser, F. Eilenberger, A. Turchanin, T. Bucher, *Adv. Funct. Mater.* **2021**, *27*, 2101086.
[6] H. Li, X. Jia, Q. Zhang, X. Wang, *Chem.* **2018**, *4*, 1510.
[7] R. J. Toh, Z. Sofer, M. Pumera, M. Pumera, *Pr. Kom. Mat.-Przyr., Poznan. Tow. Przyj. Nauk, Pr. Chem.* **2016**, *4*, 18322.
[8] Q. Yun, L. Li, Z. Hu, Q. Lu, B. Chen, H. Zhang, *Adv. Mater.* **2020**, *32*, 1903826.
[9] L. Lin, W. Lei, S. Zhang, Y. Liu, G. G. Wallace, J. Chen, *Energy Storage Mater.* **2019**, *19*, 408.
[10] F. Wu, H. Tian, Y. Shen, Z. Hou, J. Ren, G. Gou, Y. Sun, Y. Yang, T.-L. Ren, *Nature* **2022**, *603*, 259.
[11] A. Sebastian, R. Pendurthi, T. H. Choudhury, J. M. Redwing, S. Das, *Nat. Commun.* **2021**, *12*, 693.
[12] Y. Yue, J. Chen, Y. Zhang, S. Ding, F. Zhao, Y. Wang, D. Zhang, R. Li, H. Dong, W. Hu, Y. Feng, W. Feng, D. Zhang, *ACS Appl. Mater Interfaces* **2018**, *10*, 22435.
[13] Y. Zhang, F. Zhao, Y. Wang, Y. Wang, Y. Feng, W. Feng, *ACS Appl. Electron. Mater.* **2023**, *5*, 3384.
[14] E. G. Marin, D. Marian, M. Perucchini, G. Fiori, G. Iannaccone, *ACS Nano* **2020**, *14*, 1982.
[15] Z. Golsanamlou, L. Sementa, T. Cusati, G. Iannaccone, A. Fortunelli, *Adv. Theory Simul.* **2020**, *3*, 2000164.
[16] L. Tang, T. Li, Y. Luo, S. Feng, Z. Cai, H. Zhang, B. Liu, H.-M. Cheng, *ACS Nano* **2020**, *14*, 4646.
[17] J. Wang, T. Li, Q. Wang, W. Wang, R. Shi, N. Wang, A. Amini, C. Cheng, *Mater. Today Adv.* **2020**, *8*, 100098.
[18] A. K. Singh, P. Kumar, D. J. Late, A. Kumar, S. Patel, J. Singh, J. Singh, *Appl. Mater. Today* **2018**, *13*, 242.
[19] S.-S. Chee, D. Seo, H. Kim, H. Jang, S. Lee, S. P. Moon, K. H. Lee, S. W. Kim, H. Choi, M.-H. Ham, *Adv. Mater.* **2019**, *31*, 1804422.
[20] H.-J. Chuang, B. Chamlagain, M. Koehler, M. M. Perera, J. Yan, D. Mandrus, D. Tománek, Z. Zhou, *Nano Lett.* **2016**, *16*, 1896.
[21] H. Fang, S. Chuang, T. C. Chang, K. Takei, T. Takahashi, A. Javey, *Nano Lett.* **2012**, *12*, 3788.
[22] Q. Fang, X. Zhao, Y. Huang, K. Xu, T. Min, F. Ma, *J. Mater. Chem. C* **2019**, *7*, 3607.
[23] Y. Wang, R. X. Yang, R. Quhe, H. Zhong, L. Cong, M. Ye, Z. Ni, Z. Song, J. Yang, J. Shi, J. Li, J. Lu, Z. Ni, *Nanoscale* **2016**, *8*, 1179.
[24] S.-L. Li, K. Komatsu, S. Nakaharai, Y.-F. Lin, M. Yamamoto, X. Duan, K. Tsukagoshi, *ACS Nano* **2014**, *8*, 12836.
[25] H. G. Shin, H. S. Yoon, J. S. Kim, M. Kim, J. Y. Lim, S. Yu, J. H. Park, Y. Yi, T. Kim, S. C. Jun, S. Im, *Nano Lett.* **2018**, *18*, 1937.
[26] Z. Wang, M. Tripathi, Z. Golsanamlou, P. Kumari, G. Lovarelli, F. Mazziotti, D. Logoteta, G. Fiori, L. Sementa, G. M. Marega, H. G. Ji, Y. Zhao, A. Radenovic, G. Iannaccone, A. Fortunelli, A. Kis, D. Logoteta, *Adv. Mater.* **2023**, *35*, 2209371.
[27] J. Su, L. Feng, Y. Zhang, Z. Liu, *Phys. Chem. Chem. Phys.* **2016**, *18*, 16882.
[28] S. Song, Y. Sim, S.-Y. Kim, J. H. Kim, I. Oh, W. Na, D. H. Lee, J. Wang, S. Yan, Y. Liu, J. Kwak, J.-H. Chen, H. Cheong, J.-W. Yoo, Z. Lee, S.-Y. Kwon, *Nat. Electron.* **2020**, *3*, 207.
[29] L. Yang, K. Majumdar, H. Liu, Y. Du, H. Wu, M. Hatzistergos, P. Y. Hung, R. Tieckelmann, W. Tsai, C. Hobbs, P. D. Ye, *Nano Lett.* **2014**, *14*, 6275.
[30] T. Kim, Y. Kim, E. K. Kim, *Sens. Actuator A Phys.* **2020**, *312*, 112165.
[31] L. Tang, R. Xu, J. Tan, Y. Luo, J. Zou, Z. Zhang, R. Zhang, Y. Zhao, J. Lin, X. Zou, B. Liu, H.-M. Cheng, R. Zhang, *Adv. Funct. Mater.* **2021**, *31*, 2006941.
[32] M. Pandey, F. A. Rasmussen, K. Kuhar, T. Olsen, K. W. Jacobsen, K. S. Thygesen, *Nano Lett.* **2016**, *16*, 2234.
[33] Y. Guo, D. Liu, J. Robertson, *App. Phys. Lett.* **2015**, *106*, 173106.
[34] P.-C. Shen, C. Su, Y. Lin, A.-S. Chou, C.-C. Cheng, J.-H. Park, M.-H. Chiu, A.-Y. Lu, H.-L. Tang, M. M. Tavakoli, G. Pitner, X. Ji, Z. Cai, N. Mao, J. Wang, V. Tung, J. Li, J. Bokor, A. Zettl, C.-I. Wu, T. Palacios, L.-J. Li, J. Kong, *Nature* **2021**, *593*, 211.
[35] M. N. Gjerding, A. Taghizadeh, A. Rasmussen, S. Ali, F. Bertoldo, T. Deilmann, N. R. Knøsgaard, M. Kruse, A. H. Larsen, S. Manti, T. G. Pedersen, U. Petralanda, T. Skovhus, M. K. Svendsen, J. J. Mortensen, T. Olsen, K. S. Thygesen, *2D Mater.* **2021**, *8*, 044002.
[36] X. Zhao, J. Kotakoski, J. C. Meyer, E. Sutter, P. Sutter, A. V. Krasheninnikov, U. Kaiser, W. Zhou, *MRS Bull.* **2017**, *42*, 667.
[37] N. T. Trung, N. Tat, M. I. Hossain, M. I. Alam, A. Ando, O. Kitakami, N. Kikuchi, T. Takaoka, Y. Sainoo, R. Arafune, T. Komeda, *ACS Omega* **2020**, *5*, 28108.
[38] S. B. Desai, S. R. Madhvapathy, A. B. Sachid, J. P. Llinas, Q. Wang, G. H. Ahn, G. Pitner, M. J. Kim, J. Bokor, C. Hu, H.-S. P. Wong, A. Javey, *Science* **2016**, *354*, 99.
[39] B. Radisavljevic, A. Radenovic, J. Brivio, V. Giacometti, A. Kis, *Nat Nanotechnol* **2011**, *6*, 147.
[40] Y. Meir, N. S. Wingreen, *Phys. Rev. Lett.* **1992**, *68*, 2512.
[41] J.-Y. Noh, H. Kim, Y.-S. Kim, *Phys. Rev. B* **2014**, *89*, 205417.
[42] R. L. H. Freire, F. C. De Lima, A. Fazzio, *Phys. Rev. Mater.* **2022**, *6*, 084002.
[43] C. J. Mcclellan, E. Yalon, K. K. H. Smithe, S. V. Suryavanshi, E. Pop, *ACS Nano* **2021**, *15*, 1587.
[44] J. P. Perdew, K. Burke, M. Ernzerhof, *Phys. Rev. Lett.* **1996**, *77*, 3865.
[45] P. Giannozzi, S. Baroni, N. Bonini, M. Calandra, R. Car, C. Cavazzoni, D. Ceresoli, G. L. Chiarotti, M. Cococcioni, I. Dabo, A. Dal Corso, S. De Gironcoli, S. Fabris, G. Fratesi, R. Gebauer, U. Gerstmann, C. Gougoussis, A. Kokalj, M. Lazzeri, L. Martin-Samos, N. Marzari, F. Mauri, R. Mazzarello, S. Paolini, A. Pasquarello, L. Paulatto, C. Sbraccia, S. Scandolo, G. Sclauzero, A. P. Seitsonen, et al., *J. Condens. Matter Phys.* **2009**, *21*, 395502.
[46] P. Giannozzi, O. Andreussi, T. Brumme, O. Bunau, M. Buongiorno Nardelli, M. Calandra, R. Car, C. Cavazzoni, D. Ceresoli, M. Cococcioni, N. Colonna, I. Carnimeo, A. Dal Corso, S. De Gironcoli, P. Delugas, R. A. Distasio, A. Ferretti, A. Floris, G. Fratesi, G. Fugallo, R. Gebauer, U. Gerstmann, F. Giustino, T. Gorni, J. Jia, M. Kawamura, H.-Y. Ko, A. Kokalj, E. Küçükbenli, M. Lazzeri, et al., *J. Condens. Matter Phys.* **2017**, *29*, 465901.
[47] H. Joon Choi, J. Ihm, *Phys. Rev. B* **1999**, *59*, 2267.
[48] A. Smogunov, A. Dal Corso, E. Tosatti, A. Dal Corso, E. Tosatti, *Phys. Rev. B* **2004**, *70*, 045417.